J|A|C|S
ARTICLES
Published on Web 12/28/2007

Formation of Pd/Au Nanostructures from Pd Nanowires via Galvanic Replacement Reaction

Xiaowei Teng,[†] Qi Wang,[‡] Ping Liu,[†,§] Weiqiang Han,*[,†] Anatoly I. Frenkel,*[,‡] Wen Wen,[§] Nebojsa Marinkovic,[||] Jonathan C. Hanson,[§] and Jose A. Rodriguez[§]

Center for Functional Nanomaterials, Brookhaven National Laboratory, Upton, New York 11973, Department of Physics, Yeshiva University, New York, New York 10016, Department of Chemistry, Brookhaven National Laboratory, Upton, New York 11973, and Department of Chemical Engineering, University of Delaware, Newark, Delaware 19716

Received September 26, 2007; E-mail: whan@bnl.gov; anatoly.frenkel@yu.edu

Abstract: Bimetallic nanostructures with non-random metal atoms distribution are very important for various applications. To synthesize such structures via benign wet chemistry approach remains challenging. This paper reports a synthesis of a Au/Pd alloy nanostructure through the galvanic replacement reaction between Pd ultrathin nanowires (2.4 ± 0.2 nm in width, over 30 nm in length) and $AuCl_3$ in toluene. Both morphological and structural changes were monitored during the reaction up to 10 h. Continuous changes of chemical composition and crystalline structure from Pd nanowires to $Pd_{68}Au_{32}$ and $Pd_{45}Au_{55}$ alloys, and to Au nanoparticles were observed. More interestingly, by using combined techniques such as high-resolution transmission electron microscopy (HRTEM), X-ray diffraction (XRD), energy dispersive X-ray spectrometry (EDS), UV−vis absorption, and extended X−ray absorption fine structure (EXAFS) spectroscopy, we found the formation of $Pd_{68}Au_{32}$ non-random alloy with Au-rich core and Pd-rich shell, and random $Pd_{45}Au_{55}$ alloy with uniformly mixed Pd and Au atom inside the nanoparticles, respectively. Density functional theory (DFT) calculations indicated that alkylamine will strongly stabilize Pd to the surface, resulting in diffusion of Au atoms into the core region to form a non-random alloy. We believe such benign synthetic techniques can also enable the large scale preparation of various types of non-random alloys for several technically important catalysis applications.

1. Introduction

Noble metals containing bimetallic nanomaterials have been used in various technologically important areas for many years due to their unique catalytic, electronic, and magnetic properties, which differ from their monometallic counterparts.[1−3] In addition to size, shape, and chemical composition, the performance of bimetallic nanomaterials are also associated with their structural diversities to a great extent. Detailed studies of various two-metal nanostructures, such as intermetalic alloy (two metals atoms occupy special crystallographic positions within the lattice), random alloy (two metals atoms are mixed statistically in accordance with the overall concentration), non-random alloy (two metals tend to cluster within the particle, as one metal is core-rich and the other is shell-rich), or phase segregation (two metals atoms are in separated crystalline phases) are essential for their applications.[1,2,4−12]

Recently, near surface alloy (NSA) has shown promise as a catalyst design.[7,13−16] For example, Pt core-rich/Cu shell-rich NSA was made in an ultrahigh vacuum (UHV) system through the evaporation of a monolayer of Cu onto a Pt(111) single crystal at 800 K, showing a high activity toward the water−gas shift reaction with a considerable enhancement of CO−tolerance than pure Pt.[7] Since most NSAs are synthesized on a single-crystal host metal under the UHV system, it will be very important and challenging to design bimetallic alloys in the nanometer scale with non-random metal atoms distribution via benign wet chemistry approach.

[†] Center for Functional Nanomaterials, Brookhaven National Laboratory.
[‡] Department of Physics, Yeshiva University.
[§] Department of Chemistry, Brookhaven National Laboratory.
[||] Department of Chemical Engineering, University of Delaware.

(1) Somorjai, G. A. *Introduction to Surface Chemistry and Catalysis*; John Wiley & Sons: New York, 1994.
(2) Wieckoweski, A.; Savinova, E. R.; Vayenas, E. G. *Catalysis and Electrocatalysis at Nanoparticle Surface*; Marcel Dekker: New York, 2003.
(3) O'Handley, R. C. *Modern Magnetic Materials: Principles and Applications*; John Wiley & Sons: New York, 1999.
(4) Rodriguez, J. A.; Goodman, D. W. *Science* **1992**, *257*, 897−903.
(5) Scott, R. W. J.; Wilson, O. M.; Oh, S. K.; Kenik, E. A.; Crooks, R. M. *J. Am. Chem. Soc.* **2004**, *126*, 15583−15591.
(6) Chen, M. S.; Kumar, D.; Yi, C. W.; Goodman, D. W. *Science* **2005**, *310*, 291−293.
(7) Knudsen, J.; Nilekar, A. U.; Vang, R. T.; Schnadt, J.; Kunkes, E. L.; Dumesic, J. A.; Mavrikakis, M.; Besenbacher, F. *J. Am. Chem. Soc.* **2007**, *129*, 6485−6490.
(8) Maksimuk, S.; Yang, S. C.; Peng, Z. M.; Yang, H. *J. Am. Chem. Soc.* **2007**, *129*, 8684−8685.
(9) Ye, H. C.; Crooks, R. M. *J. Am. Chem. Soc.* **2007**, *129*, 3627−3633.
(10) Teng, X. W.; Yang, H. *J. Am. Chem. Soc.* **2003**, *125*, 14559−14563.
(11) Casado-Rivera, E.; Volpe, D. J.; Alden, L.; Lind, C.; Downie, C.; Vazquez-Alvarez, T.; Angelo, A. C. D.; DiSalvo, F. J.; Abruna, H. D. *J. Am. Chem. Soc.* **2004**, *126*, 4043−4049.
(12) Zhong, C. J.; Maye, M. M. *Adv. Mater.* **2001**, *13*, 1507−1511.
(13) Greeley, J.; Norskov, J. K.; Mavrikakis, M. *Annu. Rev. Phys. Chem.* **2002**, *53*, 319−348.
(14) Greeley, J.; Mavrikakis, M. *Catal. Today* **2006**, *111*, 52−58.
(15) Greeley, J.; Mavrikakis, M. *Nat. Mater.* **2004**, *3*, 810−815.
(16) Gleiter, H. *Phys. Status Solidi B-Basic Res.* **1992**, *172*, 41−51.

Among many bimetallic nanomaterials, Pd/Au is the one of the most attractive systems in catalysis research. Pd/Au has shown wide catalytic activities toward phosphoric acid fuel cell, CO/H_2 oxidation, oxidation of alcohols to aldehydes, and production of vinyl acetate monomers.[5,6,17−19] Despite the fact that various techniques have been utilized to prepare Pd, Au, Pd/Au random alloy, or core/shell nanomaterials, such as photolytic decomposition, thermal decomposition, sonochemical reduction, hydrogen reduction, polyol process, and dendrimer templating,[5,20] the synthesis of Pd/Au non-random alloy with well-controlled atomic distribution remains difficult. Since Xia and Alivisatos have developed a particle-templating approach, template-directed growth has gained significant attention due to its capability to prepare nanostructures with well-controlled dimensions and chemical compositions by selecting the templating particles (host metal) and cation (solute metal) carefully.[21] Various Ag/Au nanostructures have been made via galvanic replacement reaction by reacting sacrificial Ag template particles (with size ranges from 11 to 100 nm) with Au^{3+} compounds. The size, shape, and surface defects of the template material are shown to be the most important factors governing the final products. However, using a galvanic replacement reaction to synthesize non-random alloy structures in a size range from 2 to 3 nm, which is the favorite size range for catalysis applications in general, has not been reported.

Since the chemical and physical properties of a bimetallic system strongly depend on the heterogeneous nature of metal atoms, a combination of characterization techniques are required to decipher the *actual* structure of nanomaterials, especially when those bimetallic systems are in sub-nm to 2−3 nm size range. Extended X-ray absorption fine structure (EXAFS) spectroscopy is a well-established tool for investigating the structure of bimetallic nanomaterials, since the local environment of atoms of each resonant element can be studied separately by tuning the X-ray energy to the absorbing edge of each metal. By analyzing the EXAFS spectrum of each metal in bimetallic nanomaterials concurrently, local structural parameters (metal−metal coordination number, bond length, and their disorder) can be reliably obtained along with their uncertainties. These parameters are then used to obtain unique structural dynamics information for the binary phases. EXAFS has been successfully used to study bonding habits, geometry, and surface structures of many bimetallic nanoparticles (e.g., Pt/Ru, Pd/Cu, Pd/Au, and Pd/Se), from which the size, shape, morphology, and the short range order in atomic distributions occurring within the particles were obtained.[22] When the short range order information extracted from EXAFS analysis is combined with the knowledge of the long range order (intra-particle structure of atomic packing, particle size) and average compositional distribution within the particles obtained by complementary techniques (e.g., transmission electron microscopy (TEM), X-ray diffraction (XRD), energy dispersive X-ray spectrometry (EDS)), the *actual* structure and dynamics of nanomaterials can be quantitatively analyzed.

Herein, we present the synthesis of Pd/Au nanoalloys through the galvanic replacement reaction between Pd ultrathin nanowires (2.4 ± 0.2 nm in width, over 30 nm in length) and $AuCl_3$ in toluene in the presence of the phase transfer agent *n*-dodecyl trimethylammonium bromide (DTAB) and the capping agent octadecylamine (ODA). The changes in morphology, chemical composition, and heterogeneous structure were systematically studied by using combined techniques such as high-resolution TEM (HRTEM), XRD, EDS, ultraviolet−visible (UV−vis) absorption, and EXAFS. We observed the formation of $Pd_{68}Au_{32}$ non-random alloy with Au-rich core and Pd-rich shell, and random $Pd_{45}Au_{55}$ alloy with uniformly mixed Pd and Au atom inside the nanoparticles, respectively. From DFT calculations, alkylamine was found to be critical to form the Au core-rich/Pd shell-rich type of non-random alloy structure by inducing Pd segregating to the surface during the early stage of the reaction.

2. Methods

Galvanic Replacement Reaction between Pd Nanowires and $AuCl_3$. Pd nanowires were first synthesized by the following procedures:[20,23] Palladium nitrate (17 mg, Alfa Aesar, 99.95%) was mixed with 60 mg of *n*-dodecyl trimethylammonium bromide (DTAB, Alfa Aesar, 99%) in 5 mL of toluene. Surfactant octadecylamine (ODA, 0.4 g, Aldrich, 97%) was dissolved in 2 mL of toluene via sonication in a bath for 5 min. The dissolved palladium nitrate in the toluene mixture was then reduced through the dropwise addition of a freshly prepared solution consisting of 12 mg of sodium tetrahydridoborate ($NaBH_4$, Alfa Aesar, 99%) dissolved in 2 mL of distilled water. The color of the mixture quickly changed from brownish to black and was then left to react for 1 h at room temperature. As the reaction stopped, 2 mL of water were added to solution. After 5 min aging, the hydrophilic phase solution containing excess amounts of $NaBH_4$, if any, and phase-transfer agent (DTAB) was separated from the hydrophobic phase solution. The former solution was discarded, and the latter solution that contained as-made nanomaterials was left in the flask. At the same time, $AuCl_3$ (20 mg, Alfa Aesar, 99.9%,) was dissolved in 4 mL of toluene in the presence of 60 mg of DTAB. The mixture was then injected into fresh-made Pd nanowire solution. The reaction was conducted at room temperature up to 10 h under argon protection. Upon completion of the reaction, the product was precipitated out with ethanol, followed by centrifugation, and then redispersed in chloroform.

(17) Enache, D. I.; Edwards, J. K.; Landon, P.; Solsona-Espriu, B.; Carley, A. F.; Herzing, A. A.; Watanabe, M.; Kiely, C. J.; Knight, D. W.; Hutchings, G. J. *Science* **2006**, *311*, 362−365.
(18) Schmidt, T. J.; Jusys, Z.; Gasteiger, H. A.; Behm, R. J.; Endruschat, U.; Boennemann, H. *J. Electroanal. Chem.* **2001**, *501*, 132−140.
(19) Sennewald, K.; Glaser, H. U.S. Patent 3,761,513.
(20) Wikander, K.; Petit, C.; Holmberg, K.; Pileni, M. P. *Langmuir* **2006**, *22*, 4863−4868. (b) Narayan, A.; Landstrom, L.; Boman, M. *Appl. Surf. Sci.* **2003**, *208*, 137−141. (c) Kim, S.W.; Park, J.; Jang, Y.; Chung, Y.; Hwang, S.; Hyeon, T.; Kim, Y. W. *Nano Lett.* **2003**, *3*, 1289−1291. (d) Dhas, N. A.; Gedanken, A. J. *Mater. Chem.* **1998**, *8*, 445−450. (e) Schmid, G.; Harms, M.; Malm, J. O.; Bovin, J. O.; van Ruitenbeck, J.; Zandbergen, H. W.; Fu, W. T. *J. Am. Chem. Soc.* **1993**, *115*, 2046−2048. (f) Kan, C. X.; Cai, W. P.;Li, C. C.; Zhang, L. D.; Hofmeister, H. *J. Phys. D−Appl. Phys.* **2003**, *36*, 1609−1614. (g) Ferrer, D.; Torres-Castro, A.; Gao, X.; Sepulveda-Guzman, S.; Ortiz-Mendez, U.; Jose-Yacaman, M. *Nano Lett.* **2007**, *7*, 1701−1705.
(21) Sun, Y. G.; Xia, Y. N. *Science* **2002**, *298*, 2176−2179. (b) Sun, Y.; Mayers, B.; Xia, Y. *Adv. Mater.* **2003**, *15*, 641−646. (c) Sun, Y. G.; Mayers, B.; Xia, Y. *Nano Lett.* **2002**, *2*, 481−485. (d) Lu, X. M.; Tuan, H. Y.; Chen, J. Y.; Li, Z. Y.; Korgel, B. A.; Xia, Y. N. *J. Am. Chem. Soc.* **2007**, *129*, 1733−1742. (e) Yin, Y.; Erdonmez, C.; Shaul, A.; Alivisatos, A. P. *J. Am. Chem. Soc.* **2007**, *128*, 12671−12673.
(22) Frenkel, A. I.; Hills, C. W.; Nuzzo, R. G. *J. Phys. Chem. B* **2001**, *105*, 12689−12703. (b) Via, G. H.; Sinfelt, J. H.; Lytle, F. W. *J. Chem. Phys.* **1979**, *71*, 690−699. (c) Toshima, N.; Harada, M.; Yamazaki, Y.; Asakurat, K. *J. Phys. Chem.* **1992**, 96, 9927−9933. (d) Toshima, N.; Harada, M.; Yonezawa, T.; Kushibashi, K.; Asakurat, K. *J. Phys. Chem.* **1991**, *95*, 7448−7453. (e) Newville, M. *J. Synchrotron Rad.* **2001**, *8*, 322−324. (f) Zabinsky, S. I.; Rehr, J. J.; Ankudinov, A.; Albers, R. C.; Eller, M. J. *Phys. Rev. B.* **1995**, *52*, 2995−3009. (g) Nashner, M. S.; Frenkel, A. I.; Adler, D. L.; Shapley, J. R.; Nuzzo, R. G. *J. Am. Chem. Soc.***1997**, *119*, 7760−7771. (h) Davis, R. J.; Boudart, M. *J. Phys. Chem.* **1994**, *98*, 5471−5477. (i) Reifsnyder, S. N.; Lamb, H. H. *J. Phys. Chem. B* **1999**, *103*, 321−329. (j) Nashner, M. S.; Frenkel, A. I.; Somerville, D.; Hills, C.W.; Shapley, J. R.; Nuzzo, R. G. *J. Am. Chem. Soc.* **1998**, *120*, 8093−8101. (k) Sarkar, S. K.; Kababya, S.; Vega, S.; Cohen, H.; Woicik, J. C.; Frenkel, A. I.; Hodes, G. *Chem. Mater.* **2007**, *19*, 879−888.
(23) Teng, X.; Han, W. Q.; Ku, W.; Hücker, M. *Angew. Chem.−Int. Ed.* **2008**, in press.

Electron Microscopy. Specimens were prepared by dispersing the suspension of nanowires in chloroform (~1 mg/mL) and deposited on carbon-coated copper grids by drop-casting. HRTEM was performed using a field-emission JEM 3000FEG equipped with an EDS. Image acquisition and analysis was performed using Gatan Digital Micrograph.

X-ray Diffraction. Powder XRD spectra were obtained at beamline X7B (λ = 0.92 Å) at the National Synchrotron Light Source, Brookhaven National Laboratory, Upton, New York. The powdered samples were loaded inside quartz capillary tubes, which could be rotated during the XRD measurements to remove the preferred orientation. A Mar345 image plate detector was used to collect two-dimensional powder pattern and FIT2D code was used to integrate the powder rings.[24]

UV−Vis Absorption. UV−vis absorption spectra were collected on a Perkin-Elmer Lambda 35 spectrometer using quartz cuvettes.

EXAFS. EXAFS experiments were performed at beamline X-18B at the National Synchrotron Light Source, Brookhaven National Laboratory, Upton, New York. The storage ring energy was 2.5 GeV, and the ring current was in the range from 110 to 300 mA. A double−crystal Si (111) monochromator was used to scan X-ray energy from −150 to 1000 eV relative to Pd Kedge (24350 eV) and from −150 to 1500 eV relative to Au L_3 edge (11919 eV). Each sample (~10 mg) was prepared by drop-casting concentrated nanoparticles in chloroform solution evenly onto Kapton tape and then folding it several times for adequate uniformity and thickness for transmission EXAFS measurement. Au and Pd foils were measured in reference modes for X-ray energy calibration and data alignment. EXAFS data processing and analysis were performed using the IFEFFIT package.[22e] The passive electron reduction factors, S_0^2, were obtained to be 0.82 for Pd and 0.83 for Au by fits to the reference foils, and fixed in the analysis of the nanoparticles. The simultaneous, multiple edge (Au and Pd) analysis was employed by fitting theoretical FEFF6 signals to the experimental data in r-space.[22f] Several parameters describing electronic properties (e.g., correction to the photoelectron energy origin) and local structural environment (coordination numbers (N), bond lengths (R), and their mean-squared relative deviations σ^2) around absorbing atoms were varied in the fit. The following physically reasonable constraints were applied during the fits:

(1) The ratio of coordination numbers of Pd−Au and Au−Pd pairs must be related to the overall composition of Au and Pd in the sample:[22g] $N_{\mathrm{Pd-Au}}/N_{\mathrm{Au-Pd}} = X_{\mathrm{Au}}/X_{\mathrm{Pd}}$, where $N_{\mathrm{A-B}}$ is the coordination number of B nearest neighbors (NN) relative to A. X_{Pd} and X_{Au} are the molar concentrations of Pd and Au in the sample;

(2) The Pd−Au distance was constrained to be the same as measured from either edge: $R_{\mathrm{Pd-Au}} = R_{\mathrm{Au-Pd}}$;

(3) The bond length disorder parameters of heterogeneous metal bonds should be the same as measured from opposite atoms: $\sigma^2_{\mathrm{Pd-Au}} = \sigma^2_{\mathrm{Au-Pd}}$.

By applying these constraints, we were able to lower the total number of adjustable parameters to make it significantly smaller than the total number of relevant independent data points.

Density Functional Theory (DFT) Calculation. Calculations were performed using spin-unrestricted DFT with the DMol^3 code.[25] The Kohn−Sham one-electron equations were solved on a double numerical basis set with polarization functions (DNP, local cutoff of 5.0 Å) of accuracy comparable to a Gaussian 6-31(d) basis. Effective core potentials were used to describe the ionic cores. For all of the surfaces investigated, we used a k-point sampling of 8 × 8 × 1 Monkhorst−Pack special points in the x, y, and z directions, respectively. The exchange−correlation energy and the potential were described by the revised version of the Perdew−Burke−Ernzerhof (RPBE) functional.[26]

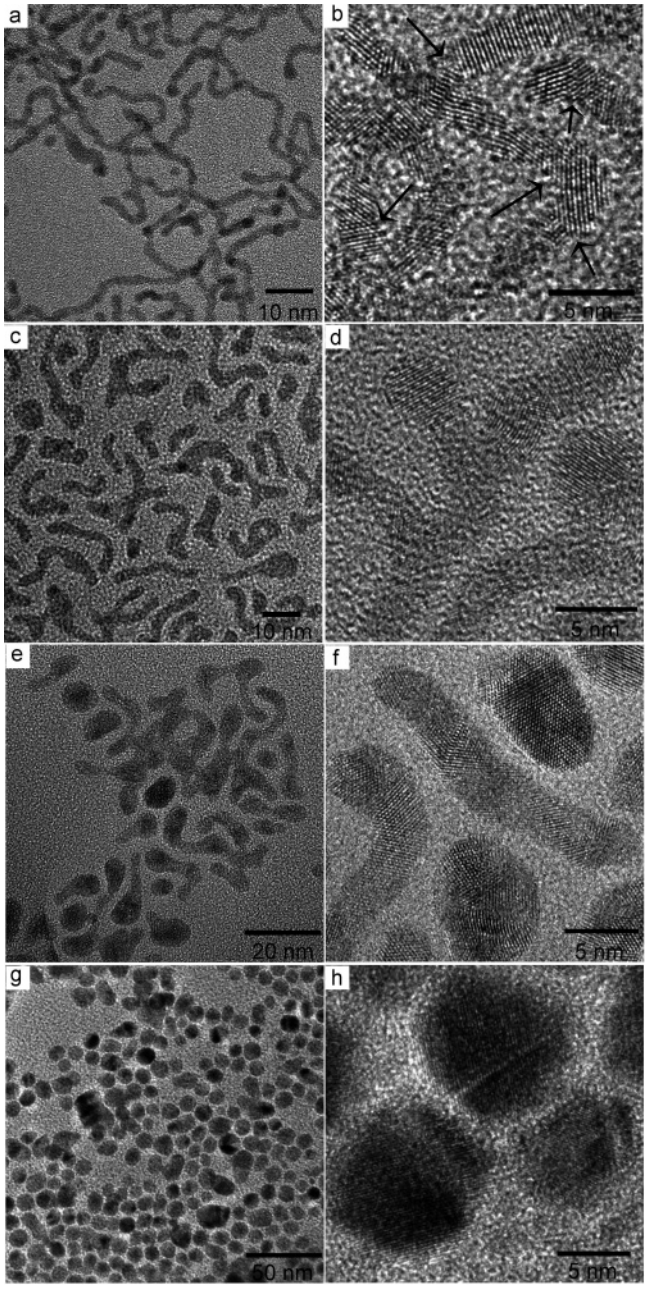

Figure 1. Morphological evolution of (a,b) Pd nanowires before and after reacting with $AuCl_3$ for (c,d) 30 min, (e,f) 2 h, and (g,h) 10 h. The arrows in (b) indicate the twinning boundaries and stacking faults in Pd nanowires.

To model Au (111) with 1 monolayer of Pd covered on the surface, Pd/Au (111), or embedded in the subsurface, Au/Pd/Au (111), we followed the 1 × 1 supercell approach with four−layer slabs with an 11-Å vacuum between the slabs. The adsorbate coverage was a monolayer. The top three layers of the surface were allowed to relax along with the adsorbates, while only the bottom layer was kept fixed at the calculated bulk lattice positions. All ofthe geometries were optimized with no symmetry constraints. The relative energy (ΔE) is defined as $\Delta E = E$(adsorbate_Pd/Au (111)) − E(adsorbate_Au/Pd/Au (111)).

3. Results and Discussion

Figures 1a and S1 (see Supporting Information) show low magnification TEM images of typical as-made Pd nanowires. The width of nanowires is uniform, with an average value of 2.4 ± 0.2 nm, and the length is in the range from 30 to 80 nm.

(24) Wang, X. Q.; Rodriguez, J. A.; Hanson, J. C.; Gamarra, D.; Martinez-Arias, A.; Fernandez-Garcia, M. *J. Phys. Chem. B* **2006**, *110*, 428−434.
(25) Delley, B. *J. Chem. Phys.* **1990**, *92*, 508−517.
(26) Hammer, B.; Hansen, L. B.; Norskov, J. K. *Phys. Rev. B* **1999**, *59*, 7413−7421.

On the basis of the HRTEM (Figure 1b), Pd nanowires are polycrystalline and composed of several single-crystalline elongated primary nanostructures (PNs). Dozens of those PNs are interconnected in a head-to-head manner via various angles to form the nanowire with a high aspect ratio (>15), while a few PNs are also connected along the nanowire to form a branch-type structure. Twinning boundaries and stacking faults, where lattice distortion and high strain are expected, are readily observed along the nanowires, especially in the location where PNs are interconnected. All of the HRTEM images show the *d* spacing to be ~2.8 Å, corresponding to (111) planes of face center cubic (fcc) Pd.

Figure 1c shows the derivative nanostructure from the galvanic replacement reaction between the ultrathin Pd nanowires and $AuCl_3$ in toluene for 30 min. The nanowires were broken into elongated nanoparticles with an average width of 2.9 ± 0.4 nm and a length of less than 30 nm. The HRTEM in Figure 1d implies that the resultant materials are also polycrystalline. However, when compared to Pd nanowires in Figure 1b, each resultant nanostructure was composed of less than ten single crystalline PNs, indicating the incomplete breakdown of Pd nanowires into elongated nanostructures with low aspect ratios (5~10). The slight increase in width indicated that a secondary growth occurred simultaneously. EDS shows the existence of Au and Pd elements with an atomic ratio of 32:68 (Figure S2, see Supporting Information), which is equivalent to that approximately 41% of the Pd ultrathin nanowires were replaced by Au, based on the fact that Pd reacts with Au^{3+} at the following formula: $3Pd + 2Au^{3+} = 3Pd^{2+} + 2Au$.

Figure 1, parts e and f, shows TEM images of Pd/Au obtained after reacting for 2 h. Nanomaterials with two types of shapes were observed: one was elongated nanoparticles and the other was nearly spherical nanoparticles with the sizes ranging from 3 to 7 nm. The elongated nanostructure was composed of 3 to 5 single crystalline PNs and its dimension was changed to 3.5 ± 0.4 nm in width and less than 20 nm in length. More interestingly, a dumbell−like structure, evident by nearly spherical shape on the tips of each particle, was observed in elongated nanoparticles. The existence of dumbell−like structure was believed to be the consequence of minimization of surface energy and had been reported during the shape evolution of elongated nanostructure.[27−29] Selected area EDS shows Au to Pd atomic ratio is 55:45, which corresponds to ~65% of the Pd ultrathin nanowires were replaced by Au.

Figure 1, parts g and h, shows TEM images of a product obtained after reacting for 10 h. All of the nanowires disappeared, and the nearly spherical nanoparticles with 10 to 15-nm diameters were observed instead. EDS spectra show only that the Au element exists in the product, indicating that Pd nanowires have been fully replaced by Au.

We further studied the crystalline structures of as-made Pd nanowires by XRD measurements (Figure 2). Well-resolved peaks were indexed as (111), (200), (220), and (311) diffraction peaks from the *Fm3m* space group. After reacting for 30 min, the resultant Pd_{68}/Au_{32} nanostructures clearly showed a phase of Pd/Au alloy with an fcc structure without signal from pure Au phase. The diffraction peaks from $Pd_{68}Au_{32}$ alloy shifted to a lower 2θ angle than that from pure Pd, indicating the increase in lattice constant of Pd due to the incorporation of Au atoms into Pd lattices; after reacting for 2 h, the Pd_{45}/Au_{55} nanostructure still showed fcc alloy structure. The diffraction peaks shifted further to an even lower 2θ angle than previous Pd and $Pd_{68}Au_{32}$ structures. After reacting for 10 h, the resultant product showed well-resolved peaks that could be assigned to fcc Au metal, which was also confirmed by EDS analysis.

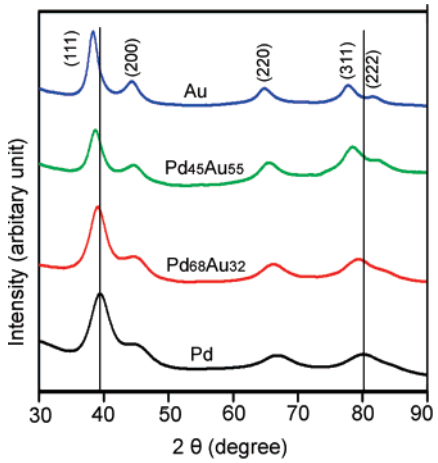

Figure 2. XRD pattern of as-made Pd, $Pd_{68}Au_{32}$, $Pd_{45}Au_{55}$, and Au nanomaterials during the galvanic replacement reaction. The data have been converted as Cu Kα radiation with wavelength of 1.54056 Å.

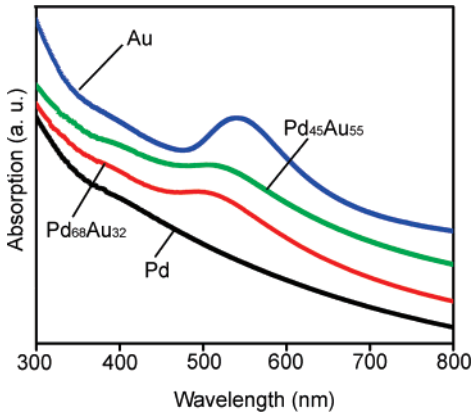

Figure 3. UV−vis absorption spectrum of as−made Pd, $Pd_{68}Au_{32}$, $Pd_{45}Au_{55}$, and Au nanomaterials.

We also performed ultraviolet−visible (UV−vis) absorption study of various Pd/Au nanostructures as shown in Figure 3. As expected, pronounced gold characteristic peaks are obtained for $Pd_{68}Au_{32}$, $Pd_{45}Au_{55}$, and Au nanostructures. With the increase in concentration of Au, the intensity of the surface plasmon resonance (SPR) peaks increased, and the SPR peak positions shifted to higher wavelength.[20g,21d] This spectroscopic evidence further confirmed the increased alloying of Au with Pd, as well as the increased overall size of the products during the reaction.

Although the crystalline structure of Pd/Au alloy structures was verified by XRD, the statistical distribution of Pd and Au atoms inside the nanoparticles, which is very crucial to the catalytic performance of Au/Pd catalysts, was not determined. Further analysis of the intra-particle structure and composition of resultant Pd/Au compounds was performed by combining EXAFS with XRD and EDS results.

(27) Son, D. H.; Hughes, S. M.; Yin, Y. D.; Alivisatos, A. P. *Science* **2004**, *306*, 1009−1012.
(28) Teng, X. W.; Yang, H. *Nano Lett.* **2005**, *5*, 885−891.
(29) Yin, Y.; Alivisatos, A. P. *Nature* **2005**, *437*, 664−670.

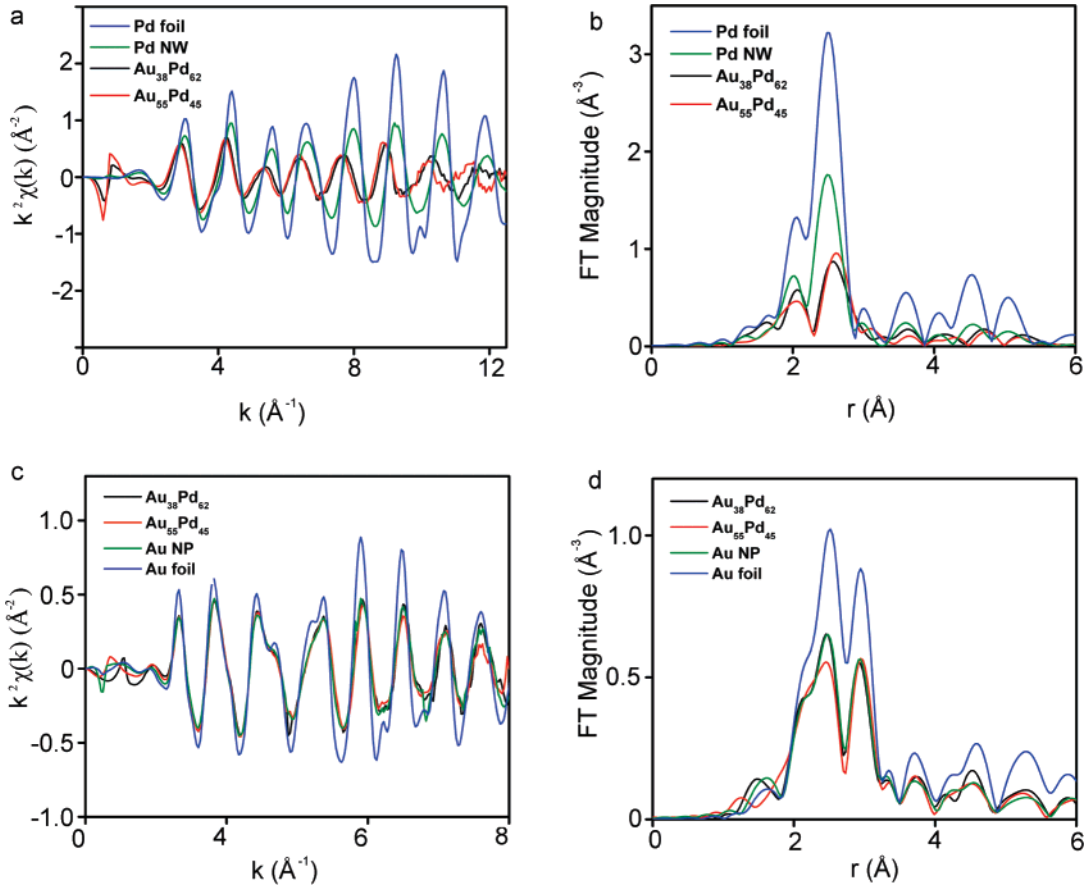

Figure 4. EXAFS data for as-made Pd nanowires, $Pd_{68}Au_{32}$, $Pd_{45}Au_{55}$, and Au nanomaterials. (a) k^2-weighted, background subtracted EXAFS signal $\chi(k)$ and (b) Fourier transform magnitudes of $k^2\chi(k)$ for Pd K-edge EXAFS; (c) (a) k^2-weighted, background subtracted $\chi(k)$ and (b) Fourier transform magnitudes of $k^2\chi(k)$ for Au L_3 edge EXAFS.

Figure 4a−d presents the raw, edge-step normalized and background subtracted EXAFS data in k- and r-spaces for all the samples measured at Pd (a, b) and Au (c, d) edges, respectively. By visually examining the Pd K-edge data, one concludes that the starting material (Pd nanowire) is similar in structure to bulk Pd, whereas some degree of alloying occurred for the rest of the samples, since they have phase shifts relative to the Pd foil and nanowire data. For the Au L_3-edge data, no phase shift relative to the bulk Au EXAFS is observed for all the three samples in their k-space data. In all cases, Pd and Au EXAFS data are clearly dominated by metal bonding. In the following sections, we will present the results of the EXAFS data analysis.

Representative fits, performed simultaneously to Au and Pd edge data for as-made Pd nanowires, $Pd_{68}Au_{32}$, $Pd_{45}Au_{55}$, and Au nanomaterials are shown in Figure 5. The best fit values of structural parameters are listed in the Table 1. As evident from Table 1, the first-nearest-neighbor (1NN) Pd−Pd coordination number N_{Pd-Pd} decreased monotonically from 9.4 (Pd nanowires) to 0 (Au nanoparticles) as the reaction progressed. Remarkably, the N_{Pd-Au} increased with reaction time faster than the X_{Au}/X_{Pd} composition ratios (N_{Pd-Au} increased from 0.3 in $Pd_{68}Au_{32}$ to 4.8 in $Pd_{45}Au_{55}$ compared to the X_{Au}/X_{Pd} increase from 32/68 to 55/45). These trends demonstrate the increased alloying in Pd/Au during the reaction. The coordination numbers of Au−Au pairs provide new and interesting information. For $Pd_{68}Au_{32}$ sample, the N_{Au-Au} was the largest (9.5), then decreased for $Pd_{45}Au_{55}$ sample down to 7.2 and then reached 8.4 for the final product (Au nanoparticles). Cumulatively, these results indicate the following sequence of local structural transformations in the sample. For the $Pd_{68}Au_{32}$ nanostructure, Au and Pd display a significant degree of segregation, in which N_{Au-Au}/N_{Au-Pd} (∼14) was obtained to be much greater (Table 1) than the ratio of the compositions X_{Au}/X_{Pd} (∼0.47) (equality would be expected for a random alloy), indicating the formation of core-shell-like non-random Pd/Au alloy during the initial stage of the replacement reaction; As the galvanic replacement reaction continued, more Au atoms entered into the Au/Pd lattice, the resultant $Pd_{45}Au_{55}$ nanostructures display the preference of random alloying, judging by the fact that N_{Au-Au}/N_{Au-Pd} (1.58) was comparable to X_{Au}/X_{Pd} (1.22); After the 10 h replacement reaction, XRD reveals that all Pd was replaced by Au^{3+}, and only Au nanoparticles were left in the system. Note that these conclusions can only be made if EXAFS, XRD, and EDX measurements are self-consistent. For example, a similar methodology was recently used by Knecht et al. in analyzing bimetallic Pd/Au nanoparticles in terms of the randomness or core-shell-like segregation of Pd and Au atoms, depending on the synthetic regimes.[30]

The following analysis allows us to discern different alloying motifs (random or core-shell-like non-random) during each stage of the reaction. For example, for $Pd_{68}Au_{32}$ elongated nanoparticles, the 1NN Pd−metal coordination number ($N_{Pd-M} \equiv N_{Pd-Au} + N_{Pd-Pd}$) was obtained to be 8.3 ± 1.0 (Table 1). However,

(30) Knecht, M. R.; Weir, M. G.; Frenkel, A. I.; Crooks, R. M. *Chem. Mater.* **2007**. (In press)

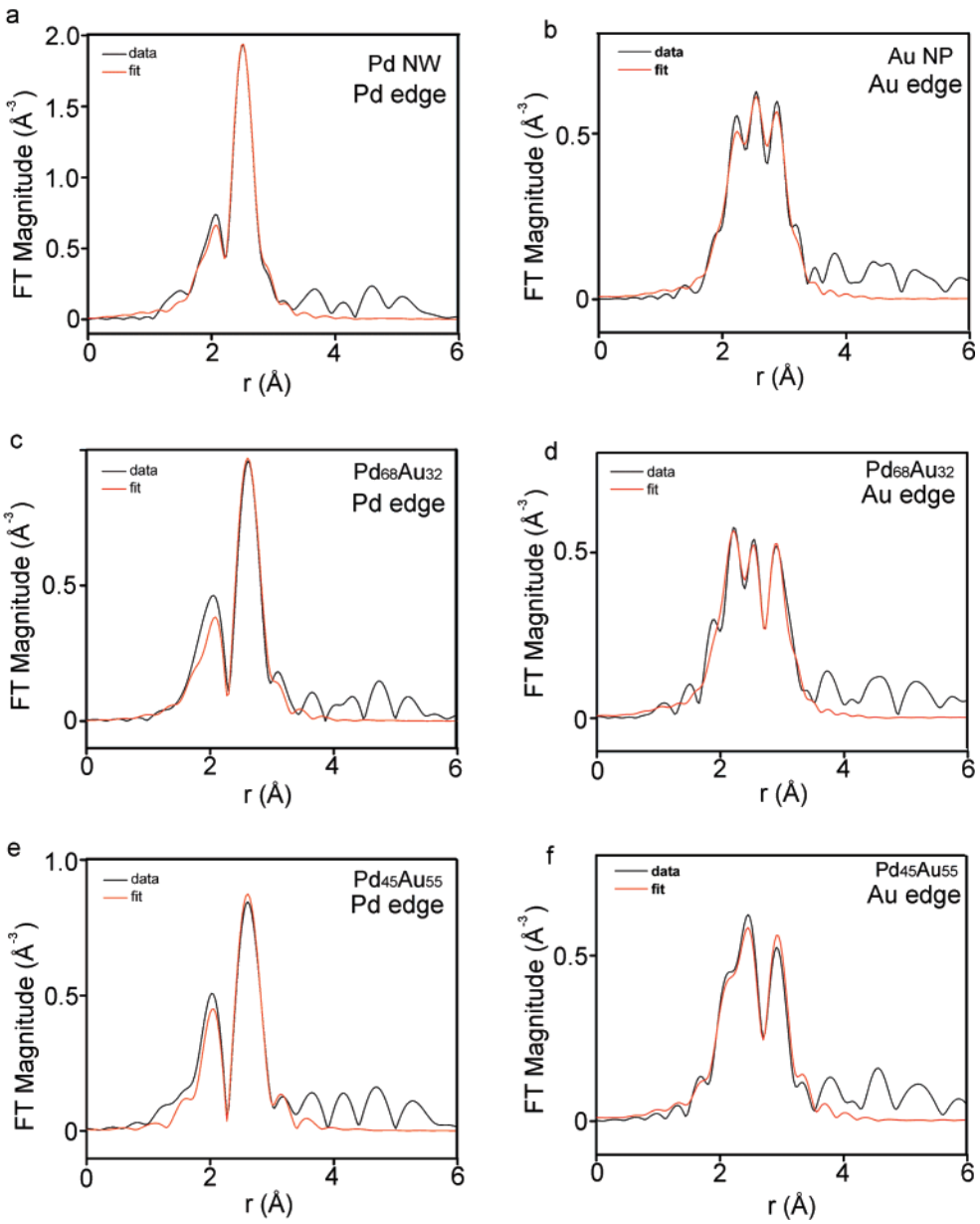

Figure 5. FT magnitudes of the data (black) and first-shell fit (red) for Pd and Au edge EXAFS. (a) Pd nanowire (NW); (b) Au nanoparticles (NP); (c, d) $Pd_{68}Au_{32}$ and (e, f) $Pd_{45}Au_{55}$.

the 1NN Au−metal coordination number (N_{Au-M}) was found to be 10.2 ± 1.5. The fact that $N_{Pd-M} < N_{Au-M}$ indicates that a large (compared to the statistical average) number of Pd atoms segregate to the surface of the elongated nanoparticles and Au to the core,[31] since atoms on the surface have fewer neighbors that those in the core.

Our analysis methodology, combining results obtained by complementary techniques, allows us to uncover the mechanism of this galvanic replacement reaction. Namely, at the beginning of the reaction (sample $Pd_{68}Au_{32}$), Au atoms enter the core of Pd nanostructure to form the Au−core rich and Pd−shell rich type of a non−random alloy. It is a very interesting and somewhat surprising result. Indeed, since the galvanic replacement reaction took place from the surface of the Pd nanowire, the resultant product was expected to be either random alloy or that with Pd-rich core and Au-rich shell.

When compared to the structure of $Pd_{68}Au_{32}$ that has been analyzed above, the structure of $Pd_{45}Au_{55}$ nanomaterials changed dramatically, as evident from EXAFS analysis. First, the Pd−M and Au−M coordination numbers were found to be consistent with 12 (corresponding to much larger nanoscale dimensions of these intermediate structures than those in the beginning of the reaction). By comparing the EXAFS and EDS data, we conclude that the random alloy was formed at the late stage of the reaction, since the value of N_{Pd-Pd}/N_{Pd-Au} was obtained to be 1.05 ± 0.37, comparable to the $X_{Pd}/X_{Au} = 0.82$.

The first-nearest-neighbor distance (R_{Pd-Pd}) of the Pd nanowire was 2.734 ± 0.009 Å (Table 1), showing slight contraction from the bulk value of 2.748 Å. In the $Pd_{68}Au_{32}$ elongated nanoparticles, the best fit value of R_{Pd-Pd} exceeded not only the R_{Pd-Au} in the same material, but also the R_{Pd-Pd} value in the bulk Pd foil. The lattice contraction (relative to the bulk) is common in metal nanoparticles and attributed to surface

(31) Frenkel, A. I. *für Krystallographie* **2007**, in press.

Table 1. Best Fit Results Obtained by EXAFS Analysis for Pd Nanowire (NW), and Bimetallic Phases Including the Final Au Nanophase (NP)[a]

sample	Pd foil	Pd NW	$Pd_{68}Au_{32}$	$Pd_{45}Au_{55}$	Au NP	Au foil
N_{Pd-Pd}	12	9.4 (4)	7.9 (1.0)	6.2 (6)		
N_{Pd-Au}			0.3 (3)	5.8 (6)		
N_{Au-Pd}			0.66 (29)[b]	4.8 (6)[b]		
N_{Au-Au}			9.5 (1.5)	7.2 (6)	8.4 (8)	12
N_{Pd-M}			8.3 (1.0)	12[c]		
N_{Au-M}			10.2 (1.5)	12[c]		
R_{Pd-Pd} (Å)	2.748 (9)	2.734 (2)	2.841 (8)	2.821 (5)		
R_{Pd-Au} (Å)			2.76 (3)	2.83 (4)		
R_{Au-Au} (Å)			2.836 (8)	2.836 (6)	2.843 (5)	2.875 (3)
σ^2_{Pd-Pd} (Å^2)	0.0055 (2)	0.0082 (3)	0.0113 (11)	0.0098 (9)		
σ^2_{Pd-Au} (Å^2)			0.006 (5)	0.032 (4)		
σ^2_{Au-Au} (Å^2)			0.0100 (14)	0.0085 (6)	0.0089 (6)	0.0080 (2)

[a] Results obtained for Pd and Au foils are listed for comparison. [b] These coordination numbers were constrained in the fits to be varied in accordance with equation: $N_{Pd-Au}/N_{Au-Pd} = X_{Au}/X_{Pd}$. Note: X_{Au}/X_{Pd} was obtained from EDS. [c] The N_{Pd-M} and N_{Au-M} are constrained to be equal to 12.

tension.[32] Qualitatively, the apparent expansion of the Pd−Pd pair distance can be attributed to Pd atoms predominantly segregating to the surface, in agreement with the independent conclusion made above by examining the metal−metal coordination numbers. Assuming a significant degree of surface relaxation that shifts Pd atoms from fcc lattice sites, one can thus qualitatively explain the experimentally observed increase in the average Pd−Pd distance relative to the bulk Pd.

A more specific mechanism of such surface relaxation is discussed here in terms of surface site vacancies. As defined by the stoichiometric relationship between Pd and Au^{3+}, three Pd atoms will be consumed to form only two Au atoms, generating a number of vacancies on the surface of template Pd nanowires. These lattice vacancies are believed to be responsible for the enhanced surface disorder qualitatively discussed above. Moreover, no lattice expansion was observed for R_{Au-Au}, indicating that Au atom environment is more ordered, presumably due to their preferential bonding in the core.

The difference of metal−metal bond length changed significantly during the reaction. As Table 1 demonstrates, all metal−metal distances in $Pd_{45}Au_{55}$ are similar in value, contrary to the trend observed in $Pd_{68}Au_{32}$. Similarity in the bond distances in $Pd_{45}Au_{55}$ is clearly consistent with the observation made independently by analyzing the coordination number trends that this system is a random alloy. The final Au nanoparticles have the bond distance relatively close to bulk Au, again consistent with the previous observation that they are reasonably large in size.

The considerable increase of the Pd−Pd bond length disorder (σ^2) in both Pd/Au alloy samples relative to that of the starting material (Pd nanowire) and bulk Pd foil points to the large structural reconstruction in the alloys, consistent with the increases of R_{Pd-Pd} in the alloy samples. In contrast, the best fit values of σ^2 of Au−Au pairs in the alloyed samples fall, considering their uncertainties, within the range of their values obtained for the final product (Au nanoparticles) and bulk Au foil. This observation indicates that Au cluster formation and growth initializes at a close vicinity to the Au fcc site location, and follows the relatively ordered evolution. This assertion, again, can be confirmed by the similarity of R_{Au-Au} between Pd/Au alloy samples and Au nanoparticles, and even bulk Au foil. As discussed in the previous section, after 2 h reaction, a randomly ordered Pd/Au alloy (sample $Pd_{45}Au_{55}$) is formed. The large value of σ^2 for Au−Pd bond for this random structure compared to that after 30 min reaction (sample $Pd_{68}Au_{32}$) in the Au-rich core and Pd-rich shell structure is one of the most interesting findings of this study. Combined with the relatively small value of the Au−Pd bond length, relative to those of Pd−Pd and Au−Au mentioned above, these results suggest that at the interface of core−shell structure formed 30 min after the beginning of the reaction, Au−Pd bonds possibly formed very stable bridges between two sublattices, ordered Au core and disordered Pd shell.

Several galvanic replacement reactions have been reported recently between various Ag nanoparticles and Au^{3+}. Depending on the size, shape, and crystalline structures of the template Ag nanoparticles, at least three different types of growth have been proposed.[20] (i) when 100 nm single crystalline Ag cubes were used, Au^{3+} preferentially adsorbs on the {110} facets, resulting in the formation of Ag/Au hollow structures; (ii) when 11 and 14 nm Ag multiple twinned particles (MTP) were used, the replacement reaction preferentially started from the {111} facets, resulting in the formation of Ag/Au hollow structures and, finally, small Au fragments; (iii) when 11 nm single crystalline Ag nanospheres (truncated cuboctahedron) were used, the replacement reaction took place on {111} facets, resulting in the formation of a Au hollow structure.

Here, we demonstrate an alternative growth mechanism between Pd nanowires and Au^{3+}. When $AuCl_3$ was injected to the solution containing ultrathin Pd nanowires, the replacement reaction started from twinning boundaries and stacking faults, instead of certain crystalline faces of Pd nanowires. These defect sites might have the highest surface energy level.[33,34] The reduced Au atoms further diffuse into the core area of the Pd nanowire to form a core Au-rich non-random Pd/Au alloy (Figure 6, Step one). Previous studies have demonstrated that the diffusion rate of Au atoms can be dramatically enhanced in the nanostructured Pd metals with the diffusion coefficient in the order of 1 nm^2/s, which is 1 order of magnitude faster than that in bulk Pd metals.[16,35] Moreover, with the presence of

(32) Frenkel, A. I.; Nemzer, S.; Pister, I.; Soussan, L.; Harris, T.; Sun, Y.; Rafailovich, M. H. *J. Chem. Phys.* **2005**, *123*, 184701.
(33) Wang, Z. L. *J. Phys. Chem. B* **2000**, *104*, 1153−1175.
(34) Xiong, Y.; Washio, I.; Chen, J.; Sadilek, M.; Xia, Y. *Angew. Chem.-Int. Ed.* **2007**, *46*, 4917−4921.
(35) Mori, H.; Komatsu, M.; Takeda, K.; Fujita, H. *Philos. Mag. Lett.* **1991**, *63*, 173−178.

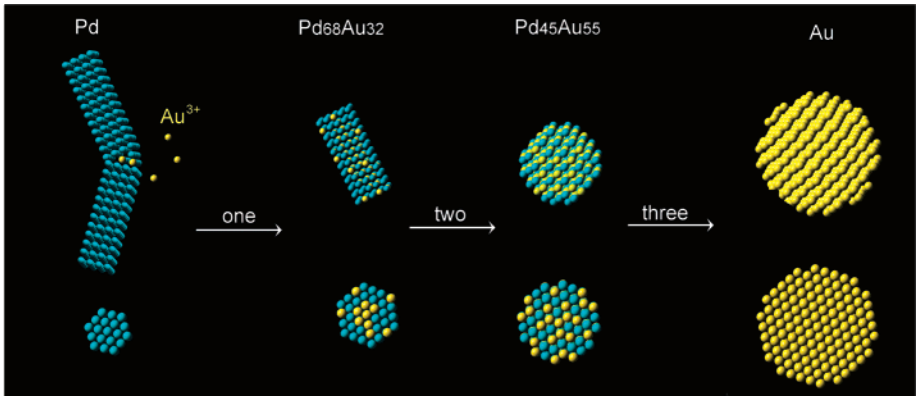

Figure 6. Schematic side view (top) and cross section (bottom) of as-made Pd, $Pd_{68}Au_{32}$, $Pd_{45}Au_{55}$, and Au nanomaterial during the galvanic replacement reaction.

vacancies, the diffusion coefficient could be enhanced even more dramatically.[35] As defined by the stoichiometric relationship between Pd and Au^{3+}, three Pd atoms will be consumed to reduce two Au cations. Therefore, a number of vacancies along the Pd nanowire were generated as the galvanic replacement reaction proceeds. Those vacancies, on one hand, would finally prompt the break−down of Pd nanowires; on the other hand, would accelerate the migration of Au atoms into the core region of the template Pd nanomaterials. Considering that the width of template Pd nanowire is only 2.4 nm, the diffusion of Au atoms into core region takes place very quickly. The nearly instantaneous diffusion process is responsible for the missing step of the observation of the structure where Au atoms are decorated on the surface of Pd nanowires. As the reaction continued, the combination of the galvanic replacement reaction (between Pd and Au^{3+}) and alloying (between Au and Pd) would go on. More Au atoms continue to add into previously formed non-random alloy and more Pd lattice positions in the shell region were occupied by Au atoms instead. The crystal structure evolved gradually from non-random alloy with core Au-rich/shell Pd-rich to the random alloy with statistically mixed Pd and Au atoms (Figure 6, Step two). Since the total Au cation concentration was equal to the molar amount of Pd nanowires, Au cations continued to etch the Pd/Au alloys by removing Pd atoms, which is the so-called dealloying process. Pd/Au alloy finally turned into pure Au particles (Figure 6, Step three).

In contrast to galvanic replacement, in which template material disappears or collapses into small fragments due to de-alloying, the Oswald ripening process results in the dissolution of small particles to facilitate the growth of large ones. We note the fact that both galvanic replacement and Oswald ripening competitively took place during the whole reaction. The former process accounts for the replacement between Pd and Au^{3+}, followed by alloying and de-alloying, resulting in chemical composition changes from Pd to Pd/Au alloys, and to the final Au nanoparticles; the latter process accounts for the growth from elongated nanostructures with 2 to 3 nm in width into final spherical particles with 10 to 15 nm diameters. In a separate experiment, we reacted Pd nanowires in the same solution, with the exception of the addition of $AuCl_3$ for up to 10 h. We found the Pd still maintained the morphology of nanowires, indicating that no Oswald ripening occurred without galvanic replacement. As long as the galvanic replacement occurred, vacancies would be generated due to the stoichiometric relationship between Pd and Au^{3+}. Since the generation of

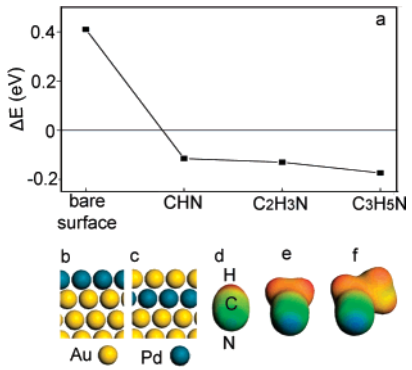

Figure 7. (a) Calculated variation of the stability of Pd on the surface of PdAu alloy at different conditions, bare surface, interacting with CHN, C_2H_3N, and C_3H_5N. (b,c) Optimized structures of Pd/Au (111) (b) and Au/Pd/Au (111) (c). (d−e) Calculated total electron density of CHN (d), C_2H_3N (e), and C_3H_5N (f) mapped by the electrostatic potential. The isosurface value is 0.05 e•Å^{-3}. Electrostatic potential is color coded as follows: blue corresponds to negatively charged regions, whereas the red represents positively charged regions.

vacancies might increase the surface energy of product dramatically, the Oswald ripening process would take place to minimize the surface energy through dissolution of Au/Pd nanostructures with small sizes and subsequent formation of nearly spherical Au/Pd particles with large sizes. In fact, the coexistence of galvanic replacement and Oswald ripening has been also found recently by reacting14 nm Ag nanoparticles with $HAuCl_4$ in solution.[21d]

To further investigate the formation of unexpected non-random $Pd_{68}Au_{32}$ alloy, we used DFT calculations to determine the thermodynamics and energetic aspects of its formation kinetics. By comparing the energies between one monolayer of Pd covered on Au surface, Pd/Au (111), or embedded in the subsurface, Au/Pd/Au (111), we were able to determine the relative energy (ΔE) as a function of chain length of adsorbates (alkylamines). Figure 7 shows that for bare surfaces corresponding to a positive ΔE, which indicates Au is more stable on the surface of Pd−Au than Pd, and Pd atoms are likely to be embedded in the bulk of Au. In contrast, with the presence of CHN, C_2H_3N, and C_3H_5N, ΔE becomes negative, indicating that there is a strong interaction between Pd and the adsorbates through the N−Pd bond to stabilize Pd on the surface. Therefore, Pd/Au (111) is preferred. In addition, with the increasing of the chain from CHN to C_3H_5N, the preferential of Pd on the surface becomes stronger. This is due to the increasing electron

accumulation at the N centers upon going from CHN to C_3H_5N, as shown (d−f), and therefore, stronger Pd−adsorbate interactions are obtained. In contrast, no interaction is observed between the alkylamines and Au in the surface, and the molecules desorb from Au/Pd/Au (111). Although calculation was done up to C_3H_5N, these trends in the relative energy (ΔE) is expected to remain practically invariant when the chain length is increased to $C_{18}H_{35}N$ (octadecylamine). These results show that a significant driving force causes Au to diffuse into Pd rather than staying in the surface layer with alkylamine in the reaction system, which is verified by EXAFS measurement as we discussed above. In fact, similar trend has been found for Mo/Au, Ni/Au and Ru/Au.[36] In those cases, Mo, Ni, or Ru atoms in the Au substrate can be pulled out to the surface by interacting with oxygen or sulfur adatoms, eventually forming oxides or sulfides.

Even though we carefully monitored the whole reaction by examining the samples at 30 min, 2 h, and 10 h during the reaction, there was no sign of forming hollow nanostructures during the reaction, in contrast to the case of the Ag template particle.[21] This might be due to the narrow width of the template Pd nanowires. In our case, nanowires with 2.4 nm widths possess high specific surface area, and consequently, high surface energy. During the galvanic reaction, a hollow structure, if any, generated within Pd nanowires would further increase the surface energy of the product. Therefore, coalescence via Ostwald ripening process will happen spontaneously to counter the increase of surface energy. In the case of Ag template particles, the size of particles is rather large (from 11 nm up to 100 nm); therefore, the resultant hollow structure may be stable and robust enough to exist during the reaction.

4. Conclusions

We have investigated the galvanic replacement reaction between ultrathin Pd nanowires and $AuCl_3$. By combined techniques such as TEM, EDS, XRD, UV−vis, and EXAFS, we found that at the early stage reaction, Au atoms preferred to segregate to core regions of the template Pd nanowire, resulting in the formation of $Pd_{68}Au_{32}$ non-random alloy with Au-rich core and Pd-rich shell. DFT calculations indicated that the addition of alkylamine stabilized Pd to the surface and cause Au atoms diffuse into the core region to form non−random alloy. As the reaction continues, more Au atoms were added in, and then the $Pd_{45}Au_{55}$ random alloy was formed with uniformly mixed Pd and Au atom inside the particles. The as-made Pd/Au non-random alloy might be extremely relevant to several technically important catalysis applications such as water gas shift reaction, CO oxidation and oxidation of alcohols to aldehydes. Considering the high reduction potential of Au^{3+} to Au ($E^{\Phi} = 1.5$ *V*), the methodology presented in this paper, in which template metals material preferentially bound with surfactant on surface react with Au^{3+} by galvanic replacement, might be used to synthesize a variety of non−random alloy systems such as Pt/Au, Ag/Au, Cu/Au, Ru/Au etc. with Au migrating to the core region. We believe such benign catalyst synthetic techniques can also enable the large-scale preparation of improved non-random alloy catalysts, avoiding using complex UHV system.

Acknowledgment. This work is supported by the U.S. Department of Energy under contract DE-AC02-98CH10886 and Laboratory Directed Research and Development Fund of Brookhaven National Laboratory (to W.H.). A.I.F. and Q.W. gratefully acknowledge the U.S. Department of Energy (DOE-BES Catalysis Science) Grant No. DE-FG02-03ER15476 for financial support of this work. Beamline X18B is supported by the NSLS, through the Divisions of Materials and Chemical Sciences of the DOE, and the Synchrotron Catalysis Consortium (U.S. DOE Grant No. DE-FG02-05ER15688).

Supporting Information Available: Low magnitude TEM image of as-made Pd nanowires (Figure S1); EDS spectra of as-made Pd nanowires and $Pd_{68}Au_{32}$, $Pd_{45}Au_{55}$ and Au nanomaterials (Figure S2); This material is available free of charge via the Internet at http://pubs.acs.org.

JA077303E

(36) Liu, P.; Rodriguez, J. A.; Muckerman, J. T.; Hrbek, J. *Phys. Rev. B* **2003**, *67*, 155416.